



# The Mechanism of Bi Nanowire Growth from Bi/Co Immiscible Composite Thin Films

Valentine V. Volobuev<sup>1,\*</sup>, Piotr Dziawa<sup>2</sup>, Alexander N. Stetsenko<sup>1</sup>, Eugene N. Zubarev<sup>1</sup>,  
Boris A. Savitskiy<sup>1</sup>, Tatyana A. Samburskaya<sup>1</sup>, Anna Reszka<sup>2</sup>,  
Tomasz Story<sup>2</sup>, and Alexander Yu. Sipatov<sup>1</sup>

<sup>1</sup>National Technical University "Kharkiv Polytechnic Institute," Frunze Street 21, Kharkiv, 61002, Ukraine,

<sup>2</sup>Institute of Physics PAS, Al. Lotnikow32/46, Warsaw, 02-668, Poland

Single crystalline Bi nanowires were grown by extrusion from Bi/Co thin films. The films were obtained by thermal evaporation in high vacuum. The average diameter, length and density of obtained nanowires were 100 nm, 30  $\mu\text{m}$  and  $6.5 \times 10^5 \text{ cm}^{-2}$ , respectively. The non-catalyzed self-organized process of whisker formation on the surface of immiscible composite thin film was exploited for nanowire growth. It was shown that the whiskers had formed during and after a thin film deposition. The value of residual stresses in a whole thin film coating as well as in its bismuth component was measured using X-ray diffraction technique. It was revealed that local compressive stresses, that had induced the whisker growth, had been formed by a segregation of Bi layers into Bi globules. A simple model of the whisker formation to minimize free energy in the Bi/Co system was proposed taking into account interfacial and elastic deformation energies. The obtained results can be utilized for growing creating of nanowires of other low-melting-point metals and semiconductors from immiscible composite thin films.

**Keywords:** Bi Nanowires, Whiskers, Stresses, Thin Films, Thermal Evaporation.

## 1. INTRODUCTION

Bi nanowires (NWs) have attracted much attention of a research community.<sup>1</sup> during the last decade. Both the large de Broglie wavelength and carrier mean free path in Bi NWs give a possibility to investigate various size-quantization effects, as well as unique transport and optical properties of one dimensional conductors.<sup>1–5</sup> Due to carrier confinement, Bi NWs have promising properties for thermoelectric applications.<sup>1,6</sup> Anomalously large magnetoresistance of Bi<sup>7–9</sup> makes possible the use Bi NWs in miniature magnetoresistive devices. The application of extruded Bi NWs as mesa-electrod interconnections has been recently demonstrated.<sup>8</sup>

In majority of previous works, Bi NWs were obtained by the top-down approach by filling alumina templates with bismuth melt under high pressure or using electrochemistry methods.<sup>1</sup> Another, bottom-up approach for the NW growth exploits a spontaneous formation of Bi whiskers on thin film surface.<sup>9,10</sup> This approach does not require the template synthesis and the NWs can be grown in a simple one-stage process by extrusion of the whiskers from a thin film.

It has been shown recently that the whiskers can be formed in thin film structures where thin film constituents are immiscible in each other, like Bi–CrN,<sup>10</sup> Bi–Cr,<sup>8</sup> Bi–Al,<sup>11,12</sup> Pb–Al,<sup>12</sup> Sn–Al,<sup>12</sup> Sn–Si.<sup>13</sup> Many aspects of the whisker formation in such systems are a subject of present and future investigations.

Nowadays, it is generally accepted that the whisker formation comes from compressive stresses<sup>14</sup> or stress gradients<sup>15</sup> in thin films. The microscopic origin of these stresses varies in different materials. The stress can arise from intermetallic compound formation accompanied by specific volume expansion<sup>14,15</sup> or due to film oxidation that stretches a thin film.<sup>16</sup> It may also originate from the difference in thermal expansion coefficients (TEC) of a thin film and a substrate<sup>9</sup> (or between thin film constituents<sup>13</sup>). In low-pressure-sputtered films intrinsic or growth-induced compressive deformations are frequently observed.<sup>17</sup> In this work, we managed to eliminate all the above mentioned reasons for compressive stress formation. We demonstrate that local compressive stress is responsible for the whisker growth in immiscible thin films and show that this stress stems from the segregation of a low melting point constituent. We present details of the Bi whisker extrusion from a composite thin film and propose a simple model to

\* Author to whom correspondence should be addressed.

explain the local compressive stress formation that induces the whisker growth.

## 2. EXPERIMENTAL DETAILS

For our study we have chosen Bi–Co system because these components are immiscible in the solid state and Bi has less than 1 at.% solubility of Co in the liquid state in temperature range 271–1000 °C.<sup>18</sup> Bi and Co have similar TECs (see Table I), thus the stress formation due to difference in TECs between the thin film components can be excluded. To eliminate the compressive stress, usually observed in sputtered condensates, and to prevent possible oxidation, we deposited the films by thermal evaporation under high vacuum conditions ( $10^{-6}$ – $10^{-7}$  Torr). Bi was thermally evaporated from a tungsten boat whereas for Co an electron gun evaporator was used. We adopted the materials alternating deposition regime usually applied for the growth of multilayers. The amount of the deposited materials was controlled during the deposition by a calibrated quartz monitor. Typical thickness of Bi and Co layers was 8.5 nm for each layer. Number of deposited layers was kept constant and was equal to 20. Insulating materials like glass, mica, polyimide, KCl (001), BaF<sub>2</sub> (111), SiO<sub>2</sub>/Si (111) and metallic foils of Ni, Cu were used as substrates. The substrates were heated from room temperature up to about 50 °C by irradiation from evaporation sources during deposition. Chromel–alumel thermocouple soldered with In to Cu and Ni foil substrates was utilized for temperature control.

Crystal structure of the obtained samples was investigated by X-ray diffraction (XRD) as well as by scanning (SEM) and transmission (TEM) electron microscopy techniques. The chemical composition of the NWs was determined by Energy Dispersive X-ray Spectroscopy (EDX) in a SEM operating in point, line, and mapping modes. The NWs were transferred onto a silicon substrate to avoid excitation of X-ray from Bi/Co thin films.

For TEM studies the NWs deposited on KCl substrate were covered with a 20-nm-thick amorphous carbon layer. For that we used a separate deposition chamber and the method of dc magnetron sputtering in Ar atmosphere. The KCl substrate was then dissolved in distilled water and the samples were collected on standard TEM grids. Placing the NW samples on the grids folded in two enabled us to observe the NWs with their axis perpendicular to electron beam (the side view) on the folded end of grids. The XRD investigations were performed in a  $\theta$ – $2\theta$  geometry using Cu-K $\alpha$  radiation.

**Table I.** Thermal expansion coefficients (TECs) at room temperature for deposited materials and substrates used in the growth of Bi nanowires.

Material	Si	Glass	Co	Ni	Bi	Cu	Polyimide	BaF <sub>2</sub>	KCl
TEC $\alpha$ , $10^{-6}$ K <sup>-1</sup>	2.27	9.5	12–13	12.5	13.4	16.4	17	18.4	36

In order to check if residual stress was present in the Bi/Co thin film two different XRD techniques were used. The first one allowed to determine the curvature of the silicon substrate by measuring the splitting of K $\alpha$  doublet diffraction maxima<sup>19</sup> before and after a thin film deposition. To determine the radius of the substrate curvature the simple relation  $R = \Delta S / \Delta\phi$  was used, where  $\Delta\phi$  is the angular difference in the splitting between K $\alpha$  doublet maxima before and after thin film deposition,  $\Delta S$  is spatial separation between two K $\alpha_1$  and K $\alpha_2$  incident beams on the sample. We slightly changed the method described in<sup>19</sup> using (110) Si monochromator and (001) Si sample substrate that allowed us to see resolved K $\alpha$  doublet in the case of large radius of substrate curvature.

The residual in-plane stress can be easily calculated by Stoney relation:

$$\sigma_F = -\frac{E_S h_S^2}{6(1-\nu_S)h_F R} \quad (1)$$

Here  $\sigma_F$  is the biaxial stress in a film,  $E_S/(1-\nu_S)$  is the biaxial Young's modulus for a substrate material,  $\nu_S$  the Poisson's ratio of a substrate material,  $R$  is the curvature radius, and  $h_S$  and  $h_F$  are the thickness of the substrate and the film, respectively.

The second method that we used to determine the stress in our films is the X-ray tensometry. Using this technique we determined interplanar distances of {024} set of Bi planes that were parallel to the film surface and tilted at  $\psi$  angle. Plotting  $\sin^2 \psi$  graph the in-plane residual stresses  $\sigma_F$  in the Bi film component can be obtained from equation:

$$\frac{(d_\psi - d_\perp)}{d} = \frac{(1+\nu)}{E} \sigma_F \sin^2 \psi \quad (2)$$

where  $(d_\psi - d_\perp)/d$  is relative change in interplanar distance along a direction tilted at  $\psi$  angle to the surface normal and along the direction is normal to a film surface,  $E$ ,  $\nu$  are Young's modulus and the Poisson's ratio of the corresponding thin film material, respectively.

## 3. RESULTS AND DISCUSSION

To check whether the whisker growth in our system can originate from a substrate–film TEC difference we have deposited Bi/Co films on various substrates with different TECs (Table I). NW formation has been observed for all the substrates conclusively proving that this mechanism is not relevant to the film–substrate TEC difference.

Beginning of the growth of whiskers was observed *in-situ* by naked eye through the window in our deposition chamber. After deposition of 10–15 layers the film surface changed from specular to matted one indicating whisker formation. Therefore, the oxidation process was not responsible for the whisker growth in the Bi/Co composite system.

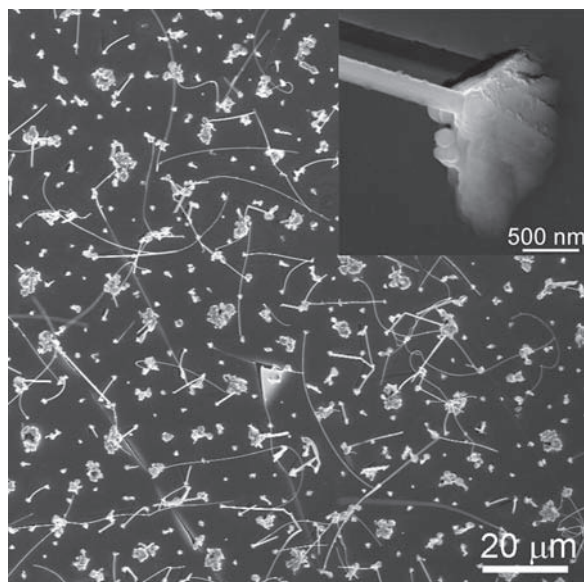


**Fig. 1.** SEM image of the Co (8.5 nm)/Bi (8.5 nm) thin film on KCl (001). The inset shows a nanowire root.

A typical SEM image of the obtained thin film condensate is presented in Figure 1. The film surface is covered with the NWs of several tens micrometers in length and hillocks with diameter of several microns. An average NW diameter was found around 100 nm. Usually, NW root lies within a hillock (see inset in Fig. 1), although some NWs originate from the film surface too. It should be noticed that most of hillocks do not finish with the NWs. Estimated density of the NWs is about  $6.5 \times 10^5 \text{ cm}^{-2}$ . Majority of the NWs possess a curved shape. A detailed SEM study of the nanowires with higher magnification reveals that the NW curvature comes from variable shape of their cross-section. Some of them are nanoribbons (Fig. 2) and can easily bend like a Möbius strip during their growth. Traces of extrusion are clearly seen on the NW surface at high magnifications (see inset in Fig. 2). Some NWs exhibit islands on their surface (Fig. 3(a), and inset in Fig. 1). That can be connected to the deposition of Bi and Co materials on the NW surface during the NW growth and

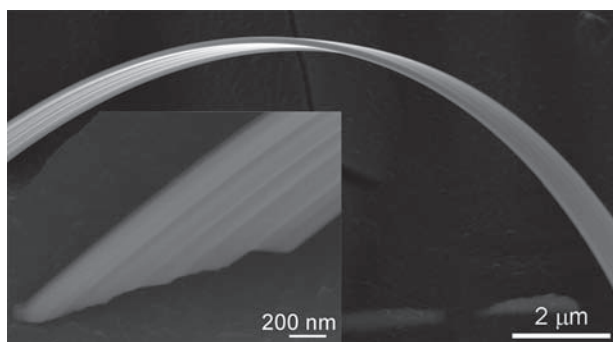


**Fig. 2.** SEM image of the part of Bi nanoribbon. The inset shows one of nanoribbon's ends.

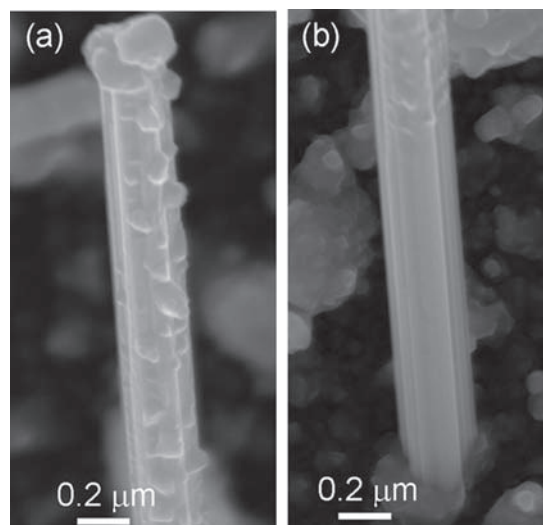


**Fig. 3.** SEM image of the top part of Bi NW (a) and the bottom part of the same NW (b).

thin film deposition. We observe NWs with and without islands. Therefore, the growth of the NWs can occur both during and after thin film deposition. Additionally, we even have observed the nanowires partially covered with islands, as it is shown in Figure 3, where, islands are seen on the top part of the NW (Fig. 3(a)), and they are absent at the bottom (Fig. 3(b)). It suggests that the top part of NW grows while the other thin film layers are being deposited but bottom part grows after the deposition has been finished.

An EDX microanalysis performed in point mode for the NWs transferred onto a silicon substrate revealed that the NWs consisted mainly of bismuth ( $99.1 \pm 0.9 \text{ at.}\%$ ). Although, there is no solubility of Co in Bi in solid state,<sup>18,20</sup> surprisingly, small amount (less than 1 at.%) of cobalt has been detected in the NWs. The presence of Co may be explained by Co deposition on the NW surface during thin film growth. Amounts of other elements (e.g., oxygen and carbon) are negligible, i.e., below the EDX measurements accuracy. More detailed information can be obtained from the EDX scans in a mapping mode (see Figs. 4(b), (c)). Both Bi and Co have nearly uniform distribution in the NW. On the tip of the NW larger amount of Co is concentrated (Fig. 4(c)). It is possible that at the beginning of the NW formation Co layer is torn and some flakes of Co are left on the tip and remain there during a subsequent NW growth. Also, an island is observed at the NW ending (Fig. 4(a)). This island as many others on NW trunk is composed basically of Bi (Fig. 4(b)).

Images of the Bi NWs with and without islands similar to the SEM ones were also obtained by TEM technique (see Fig. 5). Selected area electron diffraction (SAED) investigations showed that the obtained NWs are single crystals (see inset of Fig. 5), that is typical for whiskers. The interplanar distances obtained from the analysis of the SAED patterns match well to hexagonal Bi crystal lattice.

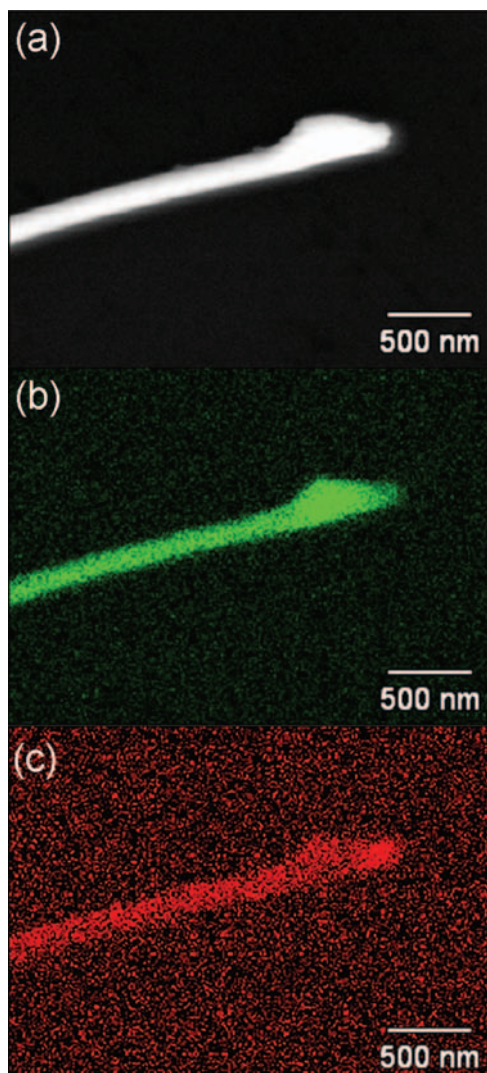


**Fig. 4.** (a) SEM image of a NW transported onto a silicon substrate. SEM-EDX elemental map of bismuth (b) and of Co (c).

The XRD spectra from the obtained thin films with the NWs show narrow diffraction maxima from Bi (Fig. 6). No preferred orientation for the Bi NWs was found. Rough estimation from Scherrer formula yielded a mean size of Bi crystallites was bigger than 30 nm. It should be noticed that the position of Bi diffraction peaks is slightly shifted to larger  $\theta$  angles that corresponds to a decrease of Bi interplanar spacing (see inset in Fig. 6). Such decrease can be related to the presence of a compressive stress in the thin film. A couple of halo observed on the XRD pattern at 28 and 44° originates from amorphous glass substrate and nanocrystalline Co, respectively. The average size of Co grains obtained from a TEM thin film investigation was found to be around 5 nm.

To inspect a residual stress level we measured the curvature of a silicon substrate by the method mentioned above, using XRD technique.<sup>19</sup> It is seen in Figure 7 that (004) Si  $K_{\alpha}$  doublet peaks slightly approach each other for the

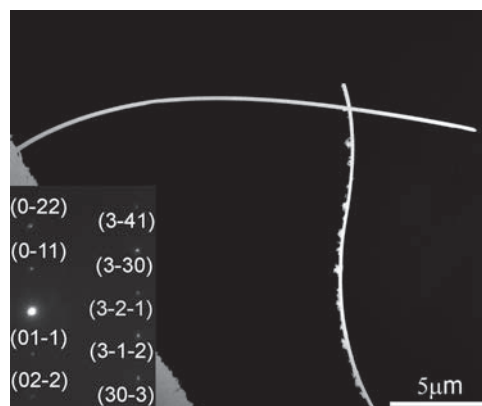


**Fig. 5.** TEM image of Bi nanowires. The inset shows {111} SAED diffraction pattern.

spectrum obtained after a thin film deposition. It means the substrate had a concave form on the side used for thin film deposition, implying a tensile stress presence in the film. A calculation using expression (1) gave us a positive in-plane stress value  $\sigma = 0.8 \pm 0.4$  GPa. On the other hand, the stresses in the film measured by X-ray tensometry occurred to be compressive. The stress value found from  $\sin^2 \psi$  graph (Fig. 8) was  $\sigma = -0.23 \pm 0.04$  GPa. The reason of such discrepancies obtained by the two methods can be understood taking into account that Bi tends to segregate in the thin film (see Fig. 9) generating particles and destroying the multilayer structure. Therefore, in the first case we determined the in-plane stress in the whole thin film but in the case of X-ray tensometry we determined the residual local in-plane stress in the Bi particles and the whiskers.

The Bi segregation comes from the large interfacial energy<sup>21</sup> that can be observed in immiscible thin film structures. Due to a large amount of broken bonds at the interface with Co, Bi attempts to saturate those bonds forming particles. The substrate temperature of 323° K is 0.6 of Bi melting temperature and it is high enough to provide Bi

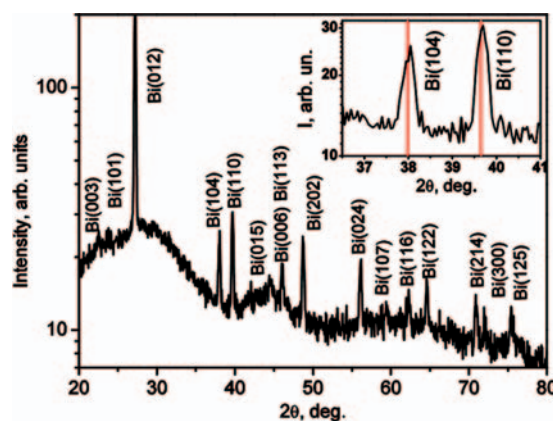


**Fig. 6.** XRD pattern of the Co (8.5 nm)/Bi (8.5 nm) thin film on glass substrate. The inset shows the shift of Bi diffraction maxima to larger  $\theta$  angles as compared to their standard crystallographic positions marked on the inset with vertical red lines.

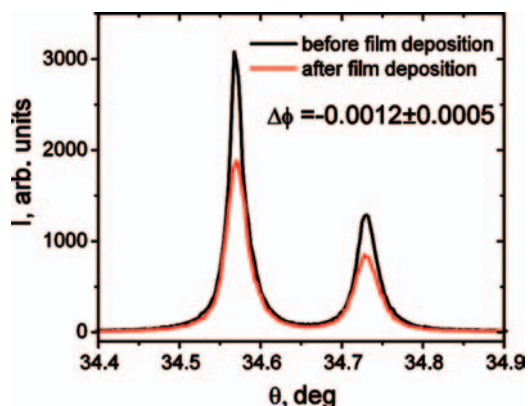


**Fig. 7.** Rocking curve of  $K_{\alpha 1}$  and  $K_{\alpha 2}$  (004) Bragg reflections of silicon substrate before and after the deposition of the Co (8.5 nm)/Bi (8.5 nm) thin film.

atoms with sufficient mobility for coalescence. For example, Bi self-diffusion coefficient  $D$  determined from grain growth<sup>22</sup> is  $1.53 \times 10^{-11} \text{ cm}^2/\text{s}$  at  $323^\circ \text{ K}$  therefore average distance that Bi atom has moved during the one hour of a thin film deposition is  $\ell = \sqrt{Dt} = 2.3 \text{ }\mu\text{m}$ . In case of Bi/Co multilayers  $D$  can be much larger due to a higher travelling speed of Bi atoms on Co surface which has no chemical bonding with Bi.

It is seen from TEM images of the Bi/Co/Bi and Co/Bi/Co samples presented in Figure 9 that the Bi segregation can be blocked by Co layers. It is necessary for Bi to stretch Co layer to form globules. As the result of the segregation, Co layers become stretched and Bi globules become compressed as observed in the stress measurement experiments.

To relate observed phenomena, namely, Bi segregation, stress formation in thin film and to explain whisker growth we propose a simple model assuming that the total free energy of the Bi/Co system  $E_{tot}$  is the sum of the interface energy  $\gamma_{int}$  and the elastic deformation energy  $\gamma_{el.def}$ :

$$E_{tot} = \gamma_{int} + \gamma_{el.def} \quad (3)$$

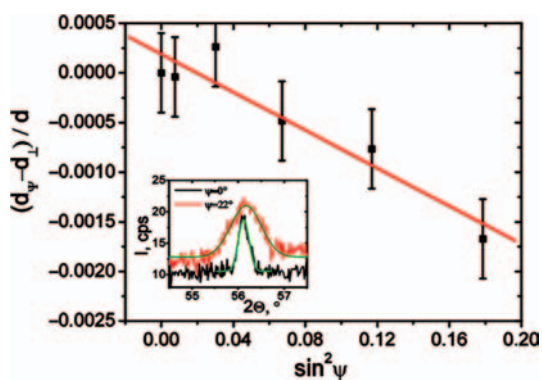


**Fig. 8.**  $\text{Sin}^2\psi$  plot for the Co (8.5 nm)/Bi (8.5 nm) thin film on a glass substrate obtained for (024) Bragg reflection of Bi. The inset shows that the position of Bi maximum is shifted when the sample is tilted at angle  $\psi$ .

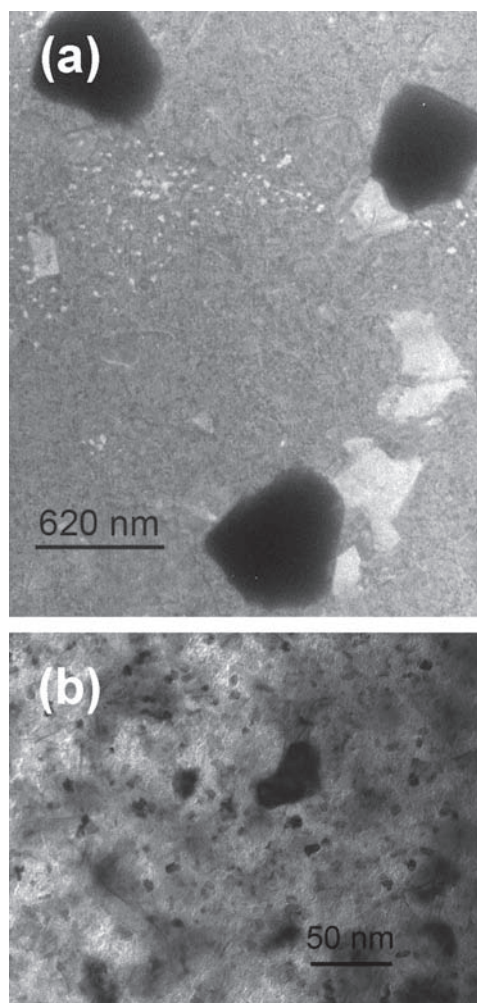


**Fig. 9.** In-plane TEM images of (a) the Bi (8.5 nm)/Co (8.5 nm)/Bi (8.5 nm) and (b) the Co (8.5 nm)/Bi (8.5 nm)/Co (8.5 nm) samples. The KCl substrate was dissolved in distilled water. Black globules correspond to Bi due to higher Bi mass-thickness contrast.

In case of the Bi/Co multilayer structure  $\gamma_{int}$  is high and the system is going to reduce it by the formation of globules from Bi layers (Figs. 10(a), (b)). The segregation process results in a stress creation in the system and increase of  $\gamma_{el.def}$  (Fig. 10(b)). This process continues until the reduction of  $E_{tot}$  from the decrease of  $\gamma_{int}$  is larger than

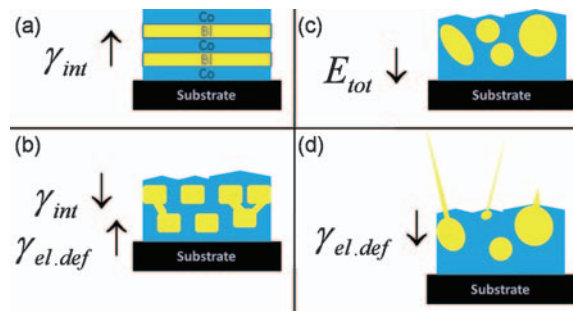


**Fig. 10.** A representative scheme of a model for Bi whisker formation.

the raise from the increase of  $\gamma_{el.def}$  (Fig. 10(c)). Then the system tends to release stresses and  $\gamma_{el.def}$ ,  $E_{tot}$  decreasing by formation of whiskers (Fig. 10(d)).

#### 4. CONCLUSIONS

Single crystalline Bi NWs were successfully fabricated by extrusion method from the Bi/Co composite thin film grown by high vacuum deposition. Details of the NW formation were studied in a model materials system of Bi/Co multilayer thin film composed of low-melting-point and high-melting-point components that are immiscible in each other. Our investigation revealed that Bi segregation in the Bi/Co composite thin film causes a local compressive stress in the bismuth component. This compressive stress is the main driving force for the NW growth. The simple model of the NW formation driven by interfacial and elastic energy minimization in the immiscible composite thin films was proposed. This model and the obtained results might be applied for fabrication of other low-melting-point metallic and semiconducting NWs.

**Acknowledgment:** Authors would like to thank Dr. E. A. Bugaev and Dr. Yu. P. Pershin from NTU “KhPI” for valuable discussions and assistance in XRD experiments.

#### References and Notes

1. M. Dresselhaus, Y. Lin, O. Rabin, M. Black, J. Kong, and G. Dresselhaus, *Nanowires*, Springer Handbook of Nanotechnology, edited by B. Bhusan, Springer, Berlin (2010), pp. 119–167.
2. M. Tian, J. Wang, Q. Zhang, N. Kumar, T. E. Mallouk, and M. H. W. Chan, *Nano Lett.* 9, 3196 (2009).
3. A. Nikolaeva, D. Gitsu, L. Konopko, M. Graf, and T. Huber, *Phys. Rev. B* 77, 075332 (2008).
4. C. Kaiser, G. Weiss, T. Cornelius, M. Toimil-Molares, and R. Neumann, *J. Phys.: Condens. Matter* 21, 205301 (2009).
5. A. Levin, M. Black, and M. Dresselhaus, *Phys. Rev. B* 79, 165117 (2009).
6. L. Hicks and M. Dresselhaus, *Phys. Rev. B* 47, 16631 (1993).
7. F. Yang, K. Liu, K. Hong, D. Reich, P. Searson, and C. Chien, *Science* 284, 1335 (1999).
8. J. Ham, J. Kang, J.-S. Noh, and W. Lee, *Nanotechnology* 21, 165302 (2010).
9. W. Shim, J. Ham, K. Lee, W. Y. Jeung, M. Johnson, and W. Lee, *Nano Lett.* 9, 18 (2008).
10. Y. T. Cheng, A. M. Weiner, C. A. Wong, M. P. Balogh, and M. J. Lukitsch, *Appl. Phys. Lett.* 81, 3248 (2002).
11. Y. W. Park, H. J. Jung, and S. G. Yoon, *Sensors and Actuators B: Chemical* 156, 709 (2011).
12. A. Santini, N. Bazzanella, N. Patel, and A. Miotello, Private communication. *E-MRS ICAM IUMRS 2011 Spring Meeting* (2011).
13. X. Xiao, A. Sachdev, D. Haddad, Y. Li, B. Sheldon, and S. Soni, *Appl. Phys. Lett.* 97, 141904 (2010).
14. N. Jadhav, E. J. Buchovecky, L. Reinbold, S. Kumar, A. F. Bower, and E. Chason, *Electronics Packaging Manufacturing, IEEE Transactions on* 33, 183 (2010).
15. M. Sobiech, M. Wohlschlögel, U. Welzel, E. Mittemeijer, W. Hügel, A. Seekamp, W. Liu, and G. Ice, *Appl. Phys. Lett.* 94, 221901 (2009).
16. M. W. Barsoum, E. N. Hoffman, R. D. Doherty, S. Gupta, and A. Zavalangos, *Phys. Rev. Lett.* 93, 206104 (2004).
17. D. Hoffman and J. A. Thornton, *J. Vac. Sci. Technol.* 20, 355 (1982).
18. K. Ishida and T. Nishizawa, *J. Phase Equilib.* 12, 346 (1991).
19. B. Cohen and M. Focht, *Solid-State Electron.* 13, 105 (1970).
20. M. Hansen and K. Anderko, *Constitution of Binary Alloys*, McGraw-Hill, New York (1958).
21. Z. Wang, J. Wang, L. Jeurgens, and E. Mittemeijer, *Phys. Rev. B* 77, 045424 (2008).
22. A. Jankowski, J. Hayes, R. Smith, B. Reed, M. Kumar, and J. Colvin, *Mater. Sci. Eng.: A* 431, 106 (2006).

Received 4 June 2011. Revised/Accepted 11 January 2012.